

Ground motion directionality in the 2010–2011 Canterbury earthquakes

Brendon A. Bradley^{1,*}† and Jack W. Baker²

¹*Department of Civil and Natural Resources Engineering, University of Canterbury, Private Bag 4800, Christchurch, New Zealand*

²*Department of Civil and Environmental Engineering, Stanford University, 473 Via Ortega, Stanford, CA, USA*

SUMMARY

This paper examines the observed directionality of ground motions in the Christchurch urban area during the 2010–2011 Canterbury, New Zealand earthquakes. A dataset of ground motions recorded at 20 strong motion stations over 10 different earthquake events is utilized to examine the ratios of various response spectral directionality definitions and the orientation of the maximum direction. Because the majority of previous related studies have utilized overlapping ground motion datasets from the NGA database, the results of this study provide a largely independent assessment of these ground motion aspects. It is found that the directionality ratio between the maximum (100th percentile) and 50th percentile orientation-independent spectral acceleration is similar to that obtained from recent studies. Ground motions from the 4 September 2010 Darfield earthquake are shown to exhibit strong directionality for source-to-site distances up to $R_{rup} = 30$ km, notably further than results from a previous study, which suggests that such effects are generally limited to $R_{rup} < 5$ km. The adopted dataset also offers the unique potential to consider site-specific effects on directionality ratios and maximum direction orientations; however, in both cases, site-specific effects are found not to be significant in the observed empirical results. Copyright © 2014 John Wiley & Sons, Ltd.

Received 6 May 2014; Revised 5 August 2014; Accepted 11 August 2014

KEY WORDS: ground motion directionality; 2010–2011 Canterbury earthquakes

1. INTRODUCTION

Earthquake-induced ground motions produce translational accelerations in two horizontal components and one vertical component. The representation of horizontal ground motion intensity via a single ground motion intensity measure (IM), which is desirable for conventional seismic design, therefore requires either some combination of the two orthogonal horizontal components, or the consideration of a single specific orientation or direction. Historically considered scalar measures include the geometric mean of the bidirectional ground motion intensity in its as-recorded orientation, the ‘larger’ of the two orientations, or a ‘random’ orientation [1–5]. Because of the dependence of the aforementioned measures on instrument orientation (the determination of which is arbitrary), Boore et al. [6] proposed that a so-called ‘orientation-independent geometric mean’ be obtained for all non-redundant orientations and then an appropriate percentile value chosen (namely the 50th or 100th percentiles, i.e. the median or maximum). Boore [7] subsequently proposed that a single component of the ground motion, rather than the geometric mean, be used in computing an orientation-independent ground motion IM. For a given ground motion, the numerical values of the above scalar definitions of a bidirectional ground motion will vary as a result of the ‘directionality’ of the ground motion.

*Correspondence to: Brendon A. Bradley, Department of Civil and Natural Resources Engineering, University of Canterbury, Private Bag 4800, Christchurch, New Zealand.

†E-mail: brendon.bradley@canterbury.ac.nz

Ground motion prediction equations (GMPEs), used in seismic hazard analysis, often provide predicted levels of ground motion intensity for a single definition of bidirectional ground motion. Historically, the use of geometric mean-based definitions have been prevalent in GMPEs [1, 8], often because of the identified fact that such definitions result in a prediction equation with marginally lower standard deviation relative to single-direction predictions. However, others have suggested that the overall seismic response of inelastic structures is more dependent on the severity of ground motion along its principal direction, and therefore propose the use of maximum direction-based definitions [9]. Although the choice of which directionality definition is most appropriate is arguably both application-specific and structure-specific, it is clearly important that the definitions used in seismic hazard and response analyses are the same in order to ensure that design and performance expectations are not biased [10, 11]. As a result, it is useful to understand the ratios of various directionality definitions so that empirical models can be developed to easily convert between available and desired definitions.

Several researchers have previously studied ground motion directionality and developed prediction models for the ratios of various directionality definitions [12–16]. Most of these studies used subsets of the NGA West or NGA West-2 databases [17], and therefore it is arguably not surprising that they yield similar empirical directionality results, and the possibility exists that such ratios may differ for other datasets.

The aim of this study is to examine ground motion directionality from the 2010–2011 Canterbury earthquake sequence. Firstly, ratios between various directionality definitions are computed using a dataset obtained from the recorded ground motions at 20 strong motion stations in Christchurch during the 10 most significant earthquakes in the 2010–2011 Canterbury earthquake sequence, a dataset that is essentially independent from those of previous studies. As well as examining the directionality ratio between the maximum component, $Sa_{RotD100}$, and the ‘average’ component, Sa_{RotD50} , so it reads additional ratios are examined with other directionality definitions, in particular, the ‘larger’ component, Sa_{Larger} , which is adopted in the current New Zealand loadings standard [9]. The potential for site-specific directionality characteristics is also examined based on the fact that the adopted dataset contains 10 repeated ground motion observations at 20 different strong motion stations.

2. GROUND MOTION DIRECTIONALITY

Various metrics for representing bidirectional horizontal ground motion intensity have been previously considered. The four metrics considered in this study are provided in Table I, while other definitions can be found in Beyer and Bommer [12]. Herein, attention is restricted to pseudo-spectral acceleration (Sa) as a ground motion IM, although much of the discussion is equally applicable to other IMs.

In examining Table I, it can be seen that two IMs represent geometric mean combinations of orthogonal horizontal components (i.e. Sa_{GM} and $Sa_{GMRotDnn}$) and while the remaining two (i.e. Sa_{Larger} and Sa_{RotDnn}) represent the ground motion in a specific orientation. It is also important to note that both Sa_{GM} and Sa_{Larger} are based on the orientation of the as-recorded ground motion components, an undesirable trait that motivated Boore et al. [6] and Boore [7] to develop the orientation-independent definitions of $Sa_{GMRotDnn}$ and Sa_{RotDnn} . For the purpose of illustration,

Table I. Ground motion directionality definitions considered in this study.

Symbol	Description
Sa_{GM}	Geometric mean of the Sa values for two as-recorded orthogonal components (H1 and H2) at each period: $Sa_{GM} = \sqrt{Sa_{H1}Sa_{H2}}$
Sa_{Larger}	Larger value of the two as-recorded components at each period: $Sa_{Larger} = \max[Sa_{H1}, Sa_{H2}]$
$Sa_{GMRotDnn}$	n -th percentile of the geometric mean value obtained by rotating the horizontal components through all non-redundant angles. Typically, the 50th and 100th (i.e. max) percentiles are considered, that is, $Sa_{GMRotD50}$ and $Sa_{GMRotD100}$, respectively.
Sa_{RotDnn}	n -th percentile of the Sa value obtained by rotating the horizontal components through all non-redundant angles. Typically, the 50th and 100th (i.e. max) percentiles are considered, that is, Sa_{RotD50} and $Sa_{RotD100}$, respectively.

Figure 1 presents the spectral response for a SDOF system with $T=2.0$ s to the Rolleston ground motion from the 4 September 2010 M_w 7.1 Darfield earthquake [18]. It can be seen from Figure 1a that the spectral response is quite polarized, with a peak displacement of nearly 35 cm along an orientation of approximately $\theta=120^\circ$ anticlockwise of the as-recorded components, and less than 20 cm at the orthogonal orientation of $\theta=30^\circ$. Figure 1b illustrates the computed values of Sa as a function of rotation angle as well as the values of the four definitions of Sa from Table I. Several important things to note in examining Figure 1b are: (i) the value of Sa at different orientations varies significantly, with the minimum and maximum values being approximately 0.18 g and 0.34 g, respectively; (ii) Sa_{Larger} is always less than or equal to the maximum value of Sa , $Sa_{RotD100}$, because it is a function of the as-recorded orientation of the instrument, which is arbitrary [6]; and (iii) although the ‘Geometric Mean’ definition of Sa , Sa_{GM} , is also a function of the as-recorded orientation of the instrument on average, it is quite similar to the median (50th percentile) value over all rotation angles, $Sa_{GMRotD50}$ [12].

2.1. The New Zealand Loadings Standard, NZS1170.5:2004

The response spectral ordinates in the New Zealand (NZ) Loadings Standard [9] are based on probabilistic seismic hazard analysis (PSHA) results obtained using the ‘Larger component’ definition of the McVerry et al. [19] (herein McV06) GMPE [9]. Since this time, the Bradley [20, 21] GMPE (herein B10) has also been incorporated into NZ PSHA for the Christchurch region following the 2010–2011 Canterbury earthquake sequence [22, 23]. The B10 GMPE was developed

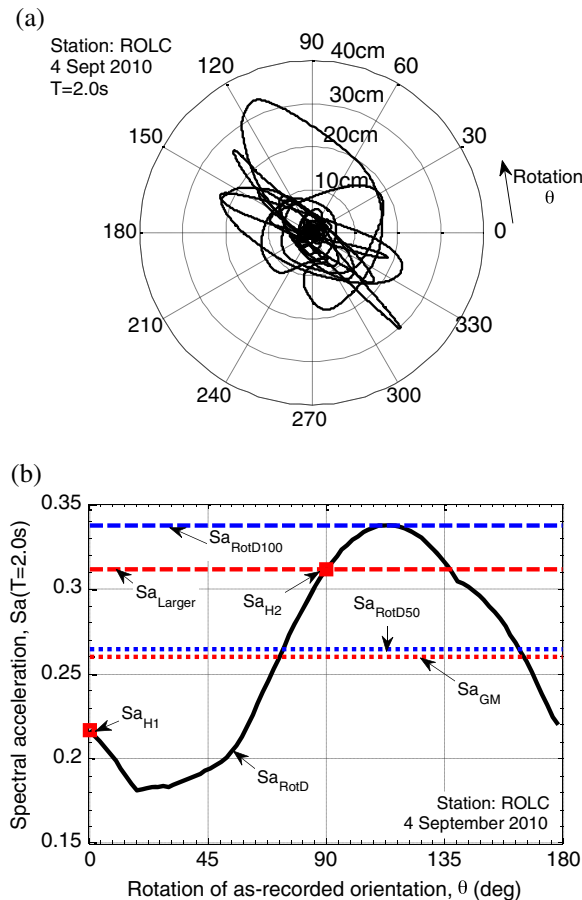


Figure 1. Directionality of the Rolleston ground motion from the 24 September 2010 M_w 7.1 Darfield earthquake: (a) Displacement response trace for a SDOF system with $T=2.0$ s; (b) Sa values obtained based on the various definitions in Table I.

from the Chiou and Youngs [24] and Chiou et al. [25] models (for $Sa_{GMROI50}$ [6]) based on geometric mean (i.e. Sa_{GM}) data from NZ. As the difference between $Sa_{GMROI50}$ and Sa_{GM} is negligible, with an average ratio of 1.0 and a lognormal standard deviation of 0.03–0.04 [12], the B10 model can arguably be considered as representing either of these Sa definitions. However, previous empirical results [e.g. 12] clearly illustrate that there is a non-negligible difference between Sa_{Larger} and Sa_{GM} , and therefore Sa values obtained directly from the B10 relationship were modified, based on the directionality ratios developed herein, for revising the seismic hazard for Christchurch.

3. OBSERVED RATIOS OF VARIOUS DIRECTIONALITY DEFINITIONS

3.1. 2010–2011 Canterbury earthquake dataset

The same set of 10 earthquake events that were recorded at 20 different strong motion stations from Bradley [26] were adopted herein to consider ground motion directionality (a total of 184 bidirectional horizontal ground motions). The location of the 10 finite faults and 20 strong motion stations is depicted in Figure 2. Seven of the ten events have a strike-slip focal mechanism, whereas the remaining three (22 Feb 2011, 23 Dec 2011 12:58 PM and 2:18 PM) have reverse mechanisms. The key attributes of this dataset are the following [26]: (i) ground motions of engineering significance, with an average PGA of 0.183 g; and (ii) multiple ground motions recorded at the same location, which allows for the consideration of site-specific ground motion directionality.

For each ground motion considered, elastic Sa amplitudes were computed based on 5% viscous damping for 20 vibration periods between $T=0.01 - 10$ s. The effect of ground motion orientation was considered by rotating all ground motions through $\theta=0 - 180^\circ$ (because the remaining orientations are redundant) with an increment of 2°



Figure 2. Location of the finite fault planes of the 10 considered earthquake events, and the location of the 20 strong motions at which directionality is examined. Color coding of the finite fault models is for clarity only. Epicentral locations of the 22 February 2011, 13 June 2011 (2:20 PM), and 23 December 2011 (1:18 PM) events are shown for the finite fault models of Beavan et al. [29] to qualitatively illustrate rupture directionality (the epicentral location of the 4 September 2011 event is beyond the figure boundaries). The six remaining events have simplified fault planes estimated based on their magnitude, fault strike and dip from moment tensor solutions, and the epicenters are therefore non-informative in this regard and not shown for clarity.

3.2. Ratio of Sa_{Larger} to Sa_{GM}

Figure 3 illustrates the computed ratio of Sa_{Larger}/Sa_{GM} for the considered ground motions as a function of vibration period. In this and subsequent figures, data points are used to illustrate the exponential of the lognormal sample mean (i.e. $\exp(\mu_{\ln X})$)—equal to the median for a lognormal distribution, which is assumed herein) of the computed ratio for all the considered ground motions, and the vertical lines are used to represent the [16th, 84th] percentile range. For comparison with the empirically-obtained ratios, the median, 16th and 84th percentiles of the model of Beyer and Bommer [12] is also provided. It can be seen that there is a small under-prediction of the empirically-obtained median by the Beyer and Bommer model; but more notably the standard deviation of the Beyer and Bommer model is significantly less than that observed for the Christchurch-specific data. As a result of these two discrepancies, a simple Christchurch-specific model was developed, which is piecewise linear in $\log T$ space, as illustrated in Figure 3. The mathematical equation for the median and standard deviation is given by Equation 1 with the coefficients given in Table II (which also provides empirical models for other directionality ratios subsequently discussed).

$$Y = \begin{cases} Y_1 & T < T_1 \\ Y_1 + (Y_2 - Y_1) \left(\frac{\ln[T/T_1]}{\ln[T_2/T_1]} \right) & T_1 \leq T < T_2 \\ Y_2 & T_2 \leq T \end{cases} \quad (1)$$

3.3. Ratio of $Sa_{RotD100}$ to Sa_{RotD50}

Figure 4 illustrates the ratio of the maximum and median values of the rotation-independent Sa , $Sa_{RotD100}/Sa_{RotD50}$, from the Christchurch-specific dataset. For comparison, the empirical prediction model of Shahi and Baker [16] is also presented, for which it can be seen that there is a very good agreement between both the median and standard deviation. The Shahi and Baker [16] model is based on the NGA West-2 dataset, comprising worldwide ground motion data from active shallow crustal earthquakes, therefore providing confidence that the Christchurch-specific results can be considered as applicable in a more general context. No practically significant dependencies on the observed directionality ratio with causal parameters (M_w , R_{rup} , etc.) was found. Note that Shahi and Baker [16] considered a R_{rup} -directionality dependence, although this resulted in only a 1% variation over a range of $R_{rup}=0-60$ km. Because of the similarity between the observed and predicted

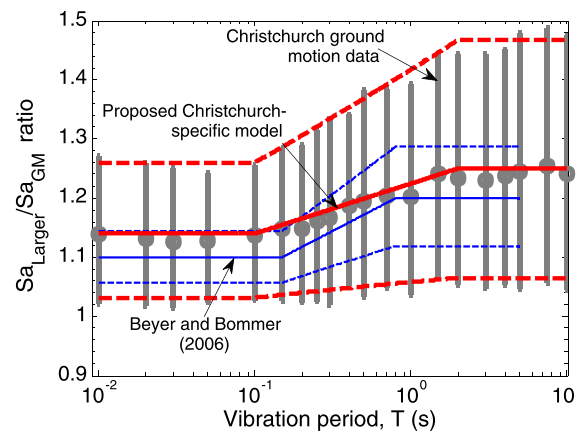


Figure 3. Ratio of Sa_{Larger} to Sa_{GM} observed as a function of vibration period. Data points represent the exponential of the lognormal sample mean, whereas the vertical bars represent the [16th, 84th] percentile range of the data. Dashed lines (red and blue) indicate model predictions of the 16th and 84th percentile range (for the Christchurch-specific model and Beyer and Bommer, respectively).

Table II. Coefficients of Christchurch-specific empirical prediction models for various directionality ratios for use in Equation 1. Median = $\exp(\mu_{lnY})$ and Std. dev = σ_{lnY} .

Ratio	$[T_1, T_2]$	$[Y_1, Y_2]$	
		Median	Std. dev
$\frac{Sa_{Larger}}{Sa_{GM}}$	[0.1, 2.0]	[1.14, 1.25]	[0.10, 0.16]
$\frac{Sa_{RotD50}}{Sa_{GM}}$	[0.1, 2.0]	[1.01, 1.06]	[0.06, 0.10]
$\frac{Sa_{RotD100}}{Sa_{Larger}}$	[0.01, 10]	[1.08, 1.08]	[0.07, 0.07]

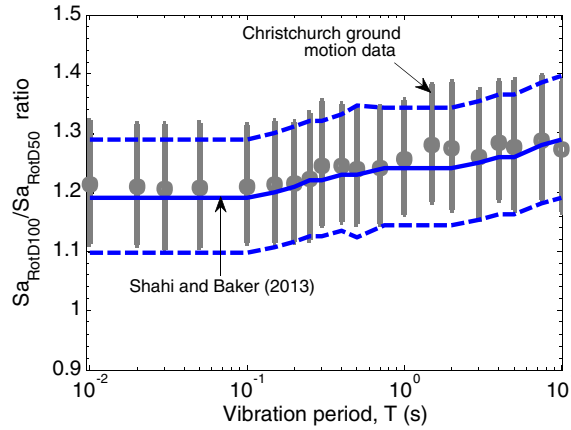


Figure 4. Ratio of $Sa_{RotD100}$ to Sa_{RotD50} observed from the Canterbury ground motion data in comparison with the model of Shahi and Baker [27] based on worldwide data.

ratios, no Christchurch-specific empirical model is provided and the model of Shahi and Baker is directly recommended.

3.4. Ratio of Sa_{RotD50} to Sa_{GM} and $Sa_{RotD100}$ to Sa_{Larger}

As previously mentioned, the current NZ loadings standard is based on the Sa_{Larger} definition; however, this definition has the limitation that it is dependent on instrument orientation. As a result, although it is the ‘larger’ of the two components in their as-recorded orientations, it is not the ‘largest’ (i.e. $Sa_{Larger} \leq Sa_{RotD100}$). For these reasons, among others, various proponents [e.g. 6] have suggested the adoption of rotation-independent measures of ground motion intensity (e.g. Sa_{RotD50} or $Sa_{RotD100}$). The aim here is not to argue which of these two orientation-independent Sa_{RotD50} metrics is more appropriate [10], but simply to develop modification factors, which would allow either Sa_{Larger} or Sa_{GM} (as computed by the McV06 and B10 GMPEs in NZ) to be converted to Sa_{RotD50} or $Sa_{RotD100}$ values.

Figure 5 illustrates the ratio of Sa_{RotD50}/Sa_{GM} obtained from the considered Christchurch dataset. The authors are not aware of previous results which have been presented for such a directionality ratio, but given the similarity of Sa_{GM} and $Sa_{GM_{Rot150}}$ [e.g. Figure 1, 12], the approximate trend of the ratio $Sa_{RotD50}/Sa_{GM_{Rot150}}$ taken from Figure 3a of Boore [7] is also provided. It can be seen that the approximate trend of Boore [7] is consistent with the obtained empirical results. Table II provides the coefficients of the Christchurch-specific prediction model presented in Figure 5.

The use of an Sa_{RotD50}/Sa_{GM} relationship allows the B10 GMPE to be used for NZ PSHA in terms of Sa_{RotD50} . Similarly, the Sa_{Larger}/Sa_{GM} and Sa_{RotD50}/Sa_{GM} relationships presented in Figures 3 and 5, respectively, can be utilized together to develop an expression Sa_{RotD50}/Sa_{Larger} , which can be used with the McV06 GMPE to provide predictions for NZ PSHA in terms of Sa_{RotD50} .

Figure 6 illustrates the ratio of $Sa_{RotD100}/Sa_{Larger}$ obtained from the considered Christchurch dataset. The authors are not aware of previous results that have been presented for such a directionality ratio for the purposes of comparison. It can be seen that the ratio is essentially independent of vibration period,

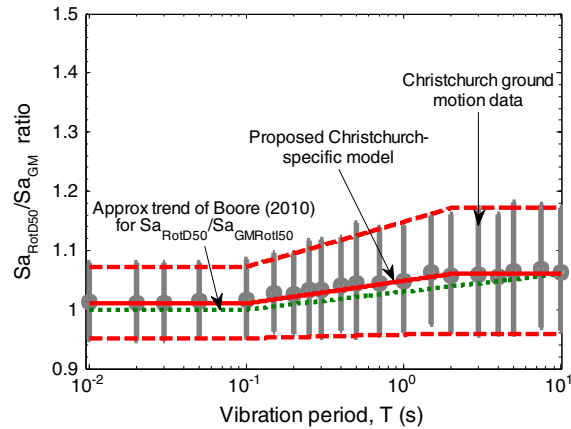


Figure 5. Ratio of Sa_{RotD50} to Sa_{GM} observed from the Canterbury ground motion data.

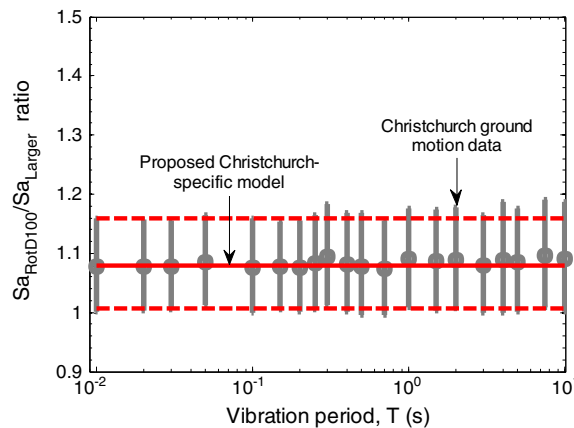


Figure 6. Ratio of $Sa_{RotD100}$ to Sa_{Larger} observed from the Canterbury ground motion data.

T , with a median value of approximately 1.08, implying that, on average, Sa_{larger} is 8% less than the maximum Sa value in any orientation (i.e. $Sa_{RotD100}$). Table II provides the coefficients of the Christchurch-specific prediction model presented in Figure 6, which represents a period-independent model with median 1.08 and lognormal standard deviation of 0.07. A constant standard deviation was pragmatically adopted, although it can be seen that there is a slight increase as T increases.

4. SITE-SPECIFIC VARIATION IN DIRECTIONALITY RATIOS

Ground motions result from the complex interaction of seismic source, path, and site effects. As noted by Shahi and Baker [16], ground motion directionality is intuitively related to the nature of the causative earthquake source rupture because of rupture directivity. However, an empirical link with source orientation is not strongly evident in observed near-fault-region directionality data [16, 27], which may point to directionality being significantly influenced by wave propagation path and site-specific effects. Because the adopted dataset contains ground motions recorded at the same set of 20 strong motion stations over 10 different earthquake events, it therefore allows, for the first time, consideration as to whether directionality can be related to site-specific conditions [26]. Herein, such site-specific directionality effects are examined for the $Sa_{RotD100}/Sa_{RotD50}$ ratio, which is directly related to ground motion polarization (i.e. having a value of 1 for unpolarized motion, and $\sqrt{2}$ for perfectly polarized motion).

Figure 7 illustrates the site-specific variations in the $Sa_{RotD100}/Sa_{RotD50}$ ratio for four different strong motion stations in comparison with the results obtained based on all ground motion data. Riccarton High School (RHSC) and Christchurch Hospital (CHHC) are gravelly and sandy soil sites located in the Canterbury basin, respectively; Heathcote Valley (HVSC) is a colluvium site located on the basin edge, which exhibited significant site effects in the Canterbury earthquakes [e.g. 18], whereas Lyttelton (LPCC) is nominally a rock site in Lyttelton Harbour [28]. For all of the sites depicted in Figure 7, it can be seen that the site-specific $Sa_{RotD100}/Sa_{RotD50}$ ratios generally show little departure from the ratios obtained based on averaging over all sites. Where deviations do exist, they are generally confined to a narrow band of vibration periods, with no consistent trend over a wide range of vibration periods. Furthermore, there is no clear evidence that the standard deviation of the ratios are notably smaller on a site-specific basis than those based on all of the strong motion stations. Similar results were observed from the remaining 16 strong motion stations not shown in Figure 7. These empirical results therefore provide evidence that polarity of ground motions shows no apparent correlation with site-specific effects.

5. DIRECTIONALITY ORIENTATION

In addition to understanding the magnitude of the directionality ratio between the average and maximum Sa directions, $Sa_{RotD100}/Sa_{RotD50}$, it is also of interest to understand the predominant orientations at which $Sa_{RotD100}$ occurs and whether this maximum direction shows any systematic tendencies at a specific site (e.g. due to polarization during wave propagation through the surficial soils and basin structure). For this purpose, the orientation of $Sa_{RotD100}$ is defined by the minimum angle with respect to the fault strike, denoted as α [16]. Using the NGA West-2 database, Shahi and Baker [27] found that α had essentially a uniform distribution (implying that the maximum direction

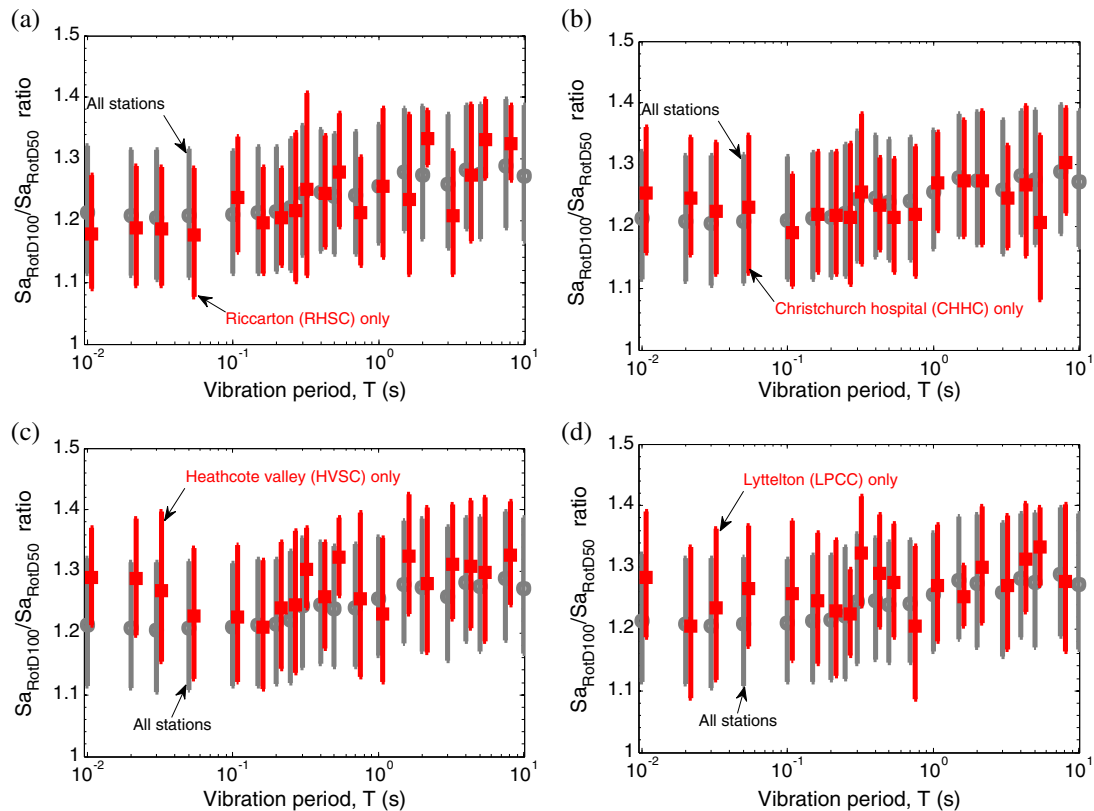


Figure 7. Examination of site-specific directionality in comparison with observations at all strong motion stations: (a) Riccarton; (b) Christchurch hospital; (c) Heathcote Valley; and (d) Lyttelton. Site-specific values have been offset on the vibration period axis for clarity.

is entirely random), with the exception of spectral ordinates for $T \geq 1$ s and source-to-site distances $R_{rup} < 5$ km. For $T \geq 1$ s and $R_{rup} < 5$ km, Shahi and Baker observed a greater likelihood that α was close to the fault-normal direction ($\alpha = 90^\circ$) than the fault-parallel direction ($\alpha = 0^\circ$), inferred to be a result of near-source rupture directivity effects (consistent with similar observations of Watson-Lamprey and Boore [13]).

Figure 8 illustrates the distribution of α for all 20 sites, 10 events, and 20 vibration periods considered in this study. It can be seen that α has essentially a uniform distribution when averaged over numerous events, source-to-site distances, and vibration periods, consistent with the findings of Shahi and Baker [27].

5.1. Event-specific variation in maximum direction orientation

Figures 9a and 9b illustrate the distribution of α for all 20 sites from the 4 September 2010 Darfield earthquake for $T < 1$ s and $T \geq 1$ s, respectively. Although Figure 9a is relatively uniform, with a slight skewness toward higher α values, it can be seen that the distribution of α in Figure 9b is highly skewed with 90% of observations having $\alpha > 45^\circ$ and 50% of observations having $\alpha > 75^\circ$. As can be seen by comparing Figures 9a and 9b, for the consideration of only moderate-to-long period spectral ordinates (i.e. $T \geq 1$) the distribution of α departs from the uniform distribution, and is more highly skewed toward $\alpha = 90^\circ$, consistent with the results of Shahi and Baker [27].

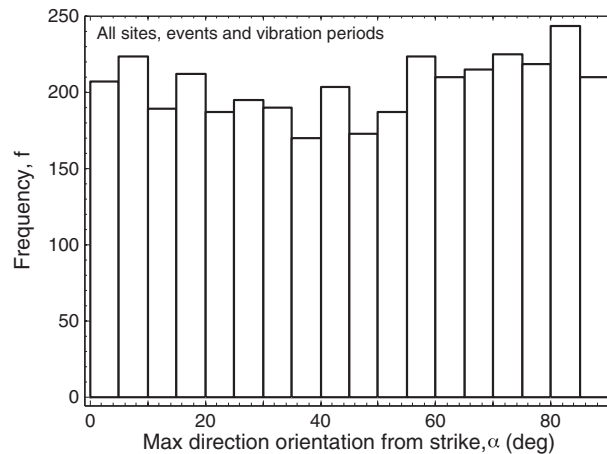


Figure 8. Histogram of the orientation of the maximum S_a direction relative to the fault strike, α , for all 20 sites, 10 events, and 20 vibration periods in the dataset.

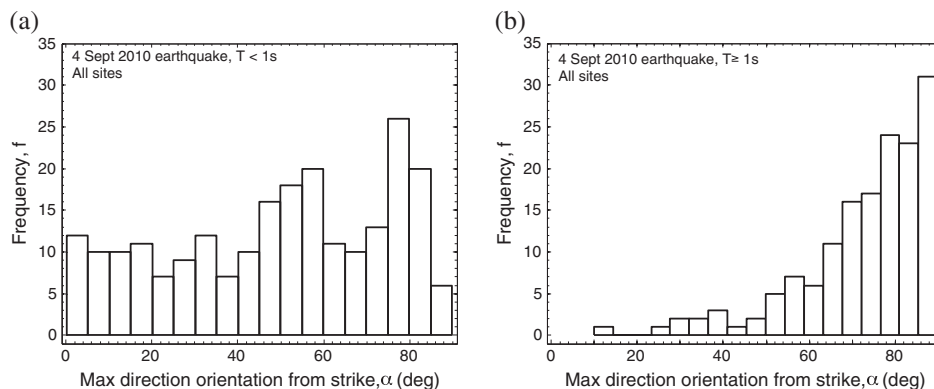


Figure 9. Histogram of the orientation of the maximum S_a direction relative to the fault strike, α , for the 4 September 2010 Darfield earthquake: (a) all sites and $T < 1$ s; and (b) all sites and $T \geq 1$ s.

Figure 10 illustrates the distribution of α values of the results in Figure 9b (i.e. $T \geq 1$ s for all 20 sites and the 4 September 2010 earthquake) as a function of source-to-site distance. In addition to showing the results for all spectral periods for $T \geq 1$ s, the average α value for a given ground motion across all the considered spectral periods (i.e. $T = 1 - 10$ s) is also shown by the bold square markers. It can be seen that the distribution of values is essentially independent of source-to-site distances over the range of $R_{rup} = 0 - 30$ km, and in fact the distribution of α in this case is most skewed toward $\alpha = 90^\circ$ for $R_{rup} \approx 15$ km. These observations are consistent with the detailed record-by-record discussion of the 4 September 2010 earthquake by Bradley [18], in which it was noted that pronounced forward directivity and basin-generated surface waves in the fault-normal direction were prevalent in the observed ground motions located to the east of the Greendale fault for distances of up to 30 km (i.e. as far north east of the causative fault as Kaiapo). These results are, however, in contrast to those presented by Shahi and Baker [27], in which the tendency for α values to be closer to the fault-normal direction ($\alpha = 90^\circ$) for $T \geq 1$ s was only noted for source-to-site distances less, $R_{rup} < 5$ km. The postulated reasons for this discrepancy are elaborated upon subsequently.

Similar to Figure 9b, Figures 11a–11c illustrate the distribution of α values for spectral periods $T \geq 1$ s from the 22 February 2011, 13 June 2011, and 23 December 2011 earthquakes, respectively. These three events and the 4 September 2010 event represent the four $M_w > 6$ earthquakes in the Canterbury earthquake sequence for which finite fault models were developed by Beavan et al. [29] (as shown in Figure 2) and adopted here. It can be seen from Figure 11 that the distribution of α for these three earthquakes is not as skewed toward $\alpha = 90^\circ$ as that for the 4 September 2010 earthquake (Figure 9b). For the 23 December 2011 earthquake, there is a slight skewness toward α values closer to the fault-normal direction; however, for the 22 February 2011 earthquake, there is notable skewness, and the 13 June 2011 event arguably is skewed toward the fault-parallel direction. Based on a record-by-record comparison, it is speculated that these observations are, at least partially, the result of the effects of rupture complexity on the observed ground motions at the 20 considered sites. In this sense, rupture complexity is considered to represent the inability of the causative faults, which were a significant contributor to the observed ground motions to be adequately represented by a planar fault structure with a uniquely defined strike angle. Such fault complexity leads to the occurrence of rupture directivity effects, which are not well aligned with the strike angle based on the single idealized planar fault. For example, Beavan et al. [29] illustrated that the 22 February 2011 earthquake was likely the result of the rupture of three principal causative faults with markedly different strike angles (as shown in Figure 2). Similarly, two, almost perpendicular, fault planes were inferred for the 13 June 2011 earthquake. The strike angle of the larger (southern) fault plane in the 13 June earthquake was considered here for the purpose of computing directionality

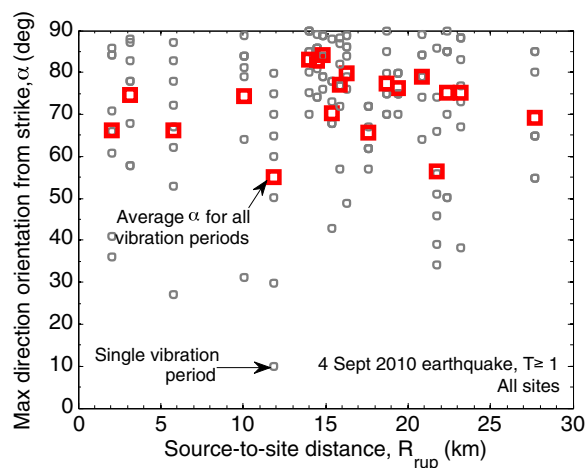


Figure 10. Variation in maximum direction orientation with source-to-site distance for the 4 September 2010 earthquake and $T \geq 1$ s. The smaller circular markers indicate α values for a single spectral period of a given ground motion, whereas the larger square markers indicate the average α value of a given ground motion cross the period range $T = 1 - 10$ s.

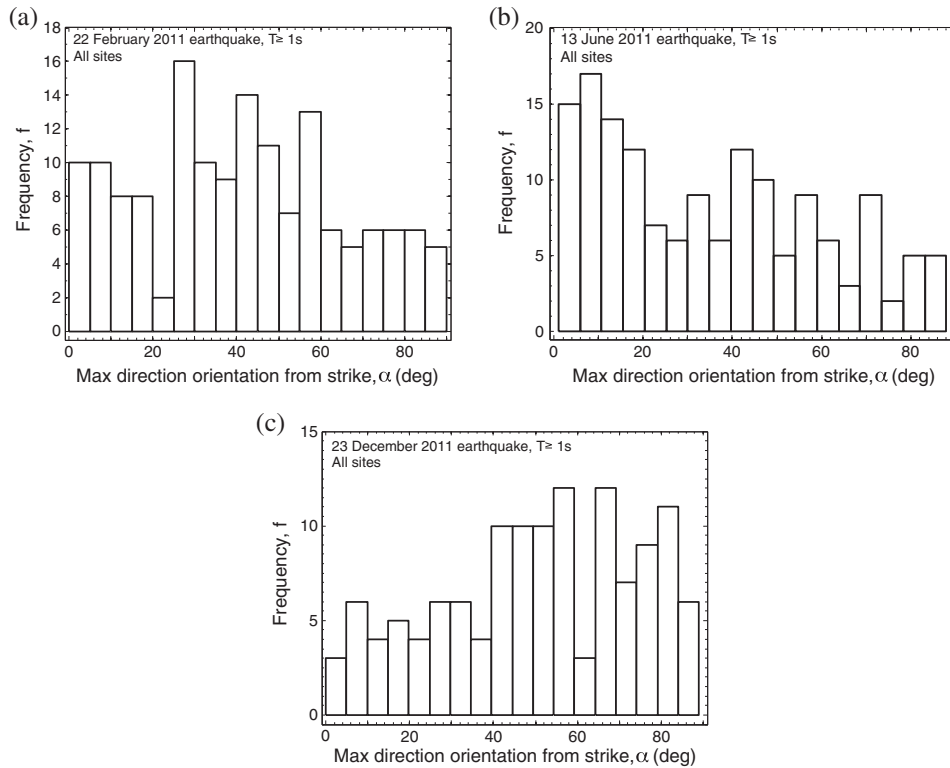


Figure 11. Histogram of the orientation of the maximum S_a direction relative to the fault strike, α , for all sites considered and $T \geq 1$ s: (a) 22 February 2011; (b) 13 June 2011; and (c) 23 December 2011 earthquakes.

orientations; however, the results in Figure 11b suggest that potentially, the northern-most fault plane contributed more significantly toward the maximum direction orientations. Although only a single fault plane was used to describe the source of the 23 December 2011 earthquake in Beavan et al. [29], it is noted by those authors that the constraint on that source inversion is relatively weak because of its location offshore. Finally, while the 4 September 2010 Darfield earthquake had arguably the most rupture complexity, with numerous non-planar fault segments [29], it is critical to note that all of the 20 sites considered here are located in the urban Christchurch region (as shown in Figure 2), and thus are located to the east of the causative faults in the region where the large slip on the Greendale fault dominates the observed ground motions (and thus the representation of this event via a single strike angle for the Greendale fault is actually relatively accurate).

The interpretation in the aforementioned paragraph is also consistent with the observation of Shahi and Baker [27] that non-uniform maximum directions were only observed at small distances. As Figure 10 illustrates, there are likely individual events in the NGA West-2 database that have strong directivity, producing non-uniform maximum directions to greater distances, but those events were presumably not well recorded, and mixed with data from many other events of varying rupture mechanism and complexity, and therefore the overall dataset shows no preferred orientation at distances greater than 5 km.

5.2. Site-specific variation in maximum direction orientation

As previously noted, the adopted dataset that contains ground motions recorded at the same set of 20 strong motion stations over 10 different earthquake events allows for the consideration as to whether directionality can be related to site-specific conditions [26, 30]. Figures 12a and 12b illustrates the variation in maximum direction orientations, ϕ , (independent of fault strike) over a 180° range of non-redundant angles at two stations for the 10 considered events; and for comparative purposes, Figure 12c illustrates the variation in maximum direction orientation from strike, α , for the 4 September 2010 earthquake at all 20 stations. Thus, these figures are intended to enable a

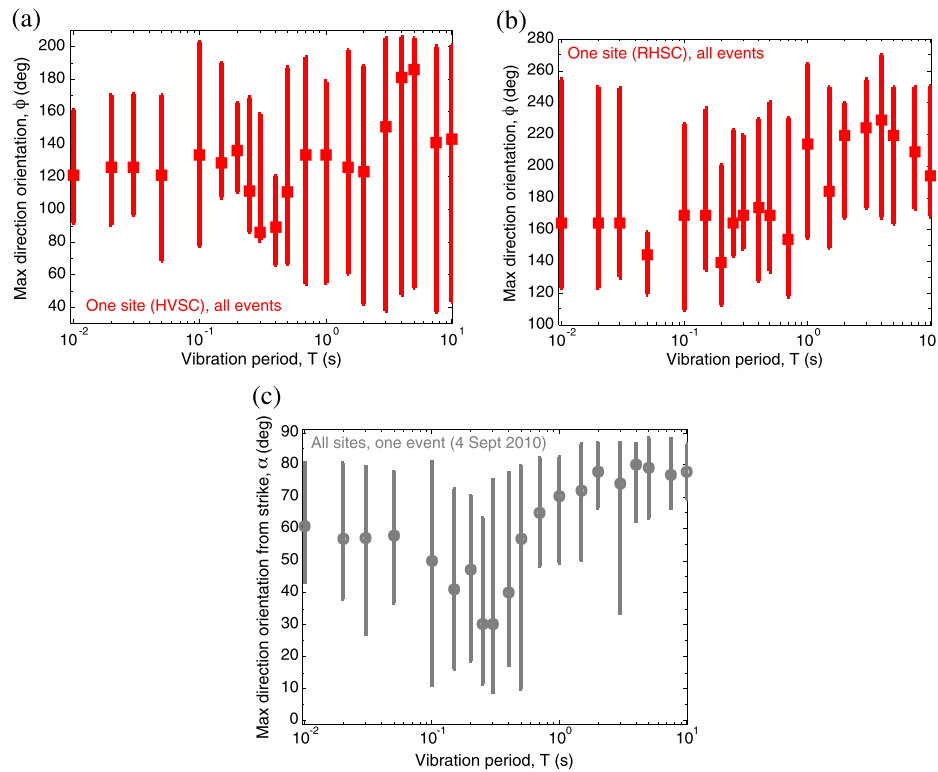


Figure 12. Comparison of the variation in the maximum direction orientation, ϕ , for all events at one site and the variation in the maximum orientation relative to fault strike, α , for all sites in one event in order to examine the significance of site-specific directionality orientation: (a) maximum direction orientation at Heathcote Valley; (b) maximum direction orientation at Riccarton High School; and (c) maximum direction orientation relative to fault strike for all sites in the 4 September 2010 event. Markers represent the median and the error bar the 16th–84th percentile range.

comparison of the significance of maximum direction orientation on a site-specific or event-specific basis. The two considered sites shown in Figure 12 are HVSC, and RHSC. The HVSC site was observed to have pronounced basin-edge effects in several of the Canterbury earthquakes [18, 28], and thus could display notable site-specific directionality, whereas the RHSC site represents a relatively typical surficial gravel site in the Canterbury basin. Figure 12a illustrates that at the HVSC station the 16th–84th percentile range on the direction of maximum spectral amplitude for $T < 0.4$ s is approximately 55 – 80° (with the exception of the 102 and 125° ranges for $T = 0.05, 0.1$ s). Despite this variability in the maximum direction orientation for $T < 0.4$ s, the median orientation of approximately 80 – 130 degrees is broadly consistent with that which would be expected because of the constructive interference of direct-S and basin-diffracted Rayleigh waves from the basin edge immediately to the east of the HVSC station. In contrast with the aforementioned observations at short periods, it can be seen that for $T > 0.4$ s there is significant variability in the maximum direction orientations (16th–84th percentile ranges on the order of 120° , which would be expected for a random orientation distribution). At the RHSC station, as shown in Figure 12b, there is generally significant variability in the maximum direction orientation, with the reason for the one exception for $T = 0.05$ s unclear.

A comparison of Figures 12a and 12b with Figure 12c clearly illustrates that at long periods the variation in the directionality ratios is larger for the site-specific cases compared with an event-specific case. This implies that, at long periods, maximum direction orientations are on average more closely aligned with the characteristics of the fault as opposed to site-specific properties. In contrast, the observations in Figure 12 illustrate the potential for site-specific effects on maximum direction orientations resulting from topographic features in the shallow surficial stratigraphy to manifest at shorter vibration periods.

6. CONCLUSIONS

This paper has examined the directionality of ground motions observed at 20 strong motion stations in the Christchurch urban area during the 10 most notable events in the 2010–2011 Canterbury earthquake sequence. Directionality ratios between various directionality definitions were computed and compared with existing models. Such comparisons are insightful in the sense that the majority of previous such studies have utilized largely overlapping datasets from the NGA database (which also has few stations with multiple observed strong motions), and thus the comparisons in this study provide insight into the possibility that such ratios may be region (or even site) dependent.

It was found that the directionality ratio between the maximum (100th percentile) and 50th percentile orientation-independent spectral acceleration, $Sa_{RotD100}/Sa_{RotD50}$ was similar to that obtained from the recent work of Shahi and Baker [16] using ground motions from the NGA West-2 database. Ground motions from the 4 September 2010 Darfield earthquake were shown to exhibit strong polarity for source-to-site distances up to $R_{rup} = 30$ km, notably further than results of Shahi and Baker [16], which suggests that such effects are generally limited to $R_{rup} < 5$ km. Based on examination of the maximum direction orientations for other events in the Canterbury earthquake sequence it was argued that the variability in the maximum direction orientation was largely a function of the adequacy of the use of a single finite fault to define the unique fault strike direction, and thus complex fault ruptures exhibit greater variability in the maximum direction orientation.

The adopted dataset also offered the potential to consider site-specific effects on directionality ratios and maximum direction orientations. For several sites, the directionality ratios were observed to vary slightly from those obtained based on all sites; however, such variations were observed to occur over a narrow band of periods. Finally, site-specific deviation in maximum direction orientations were observed to be insignificant for the empirical results examined in comparison to the dependence on a single event (i.e. source-specific effects).

ACKNOWLEDGEMENTS

Financial support provided by the New Zealand Ministry of Business, Innovation and Employment and the New Zealand Earthquake Commission are greatly appreciated. David Boore provided constructive comments that improved the paper.

REFERENCES

1. Douglas J. Earthquake ground motion estimation using strong motion records: a review of equations for the estimation of peak ground acceleration and response spectral ordinates. *Earth Science Reviews* 2003; **61**:43–104.
2. Boore DM, Joyner WB, Fumal TE. Equations for estimating horizontal response spectra and peak acceleration from Western North American Earthquakes: a summary of recent work. *Seismological Research Letters* 1997; **68**(1):128–153. DOI: 10.1785/gssrl.68.1.128
3. Abrahamson NA, Silva WJ. Empirical response spectral attenuation relations for shallow crustal earthquakes. *Seismological Research Letters* 1997; **68**(1):94–127. DOI: 10.1785/gssrl.68.1.94
4. Campbell KW. Empirical near-source attenuation relationships for horizontal and vertical components of peak ground acceleration, peak ground velocity, and pseudo-absolute acceleration response spectra. *Seismological Research Letters* 1997; **68**(1):154–179. DOI: 10.1785/gssrl.68.1.154
5. Sadigh K, Chang C-Y, Egan JA, Makdisi F, Youngs RR. Attenuation relationships for shallow crustal earthquakes based on California strong motion data. *Seismological Research Letters* 1997; **68**(1):180–189. DOI: 10.1785/gssrl.68.1.180
6. Boore DM, Watson-Lamprey J, Abrahamson NA. Orientation-independent measures of ground motion. *Bulletin of the Seismological Society of America* 2006; **96**(4A):1502–1511. DOI: 10.1785/0120050209
7. Boore DM. Orientation-independent, nongeometric-mean measures of seismic intensity from two horizontal components of motion. *Bulletin of the Seismological Society of America* 2010; **100**(4):1830–1835. DOI: 10.1785/0120090400
8. Abrahamson NA, Atkinson GM, Boore DM, Bozorgnia Y, Campbell KW, Chiou B, Idriss IM, Silva WJ, Youngs RR. Comparisons of the NGA ground-motion relations. *Earthquake Spectra* 2008; **24**(1):45–66
9. NZS 1170.5. *Structural design actions, Part 5: Earthquake actions - New Zealand*. Standards New Zealand: Wellington, New Zealand, 2004; 82.
10. Stewar JP, Abrahamson N, Atkinson GM, Baker JW, Boore DM, Bozorgnia Y, Campbell KW, Comartin CD, Idriss IM, Lew M, Mehrain M, Moehle JP, Naeim F, Sabol TA. Representation of bidirectional ground motion for design spectra in building codes. *Earthquake Spectra* 2011; **27**(3):927–937.
11. Baker JW, Cornell CA. Which spectral acceleration are you using? *Earthquake Spectra* 2006; **22**(2):293–312.

12. Beyer K, Bommer JJ. Relationships between median values and between aleatory variabilities for different definitions of the horizontal component of motion. *Bulletin of the Seismological Society of America* 2006; **96**(4A):1512–1522. DOI: 10.1785/0120050210
13. Watson-Lamprey JA, Boore DM. Beyond SaGMRotI: Conversion to SaArb, SaSN, and SaMaxRot. *Bulletin of the Seismological Society of America* 2007; **97**(5):1511–1524. DOI: 10.1785/0120070007
14. Campbell KW, Bozorgnia Y. NGA Ground motion model for the geometric mean horizontal component of PGA, PGV, PGD and 5% damped linear elastic response spectra for periods ranging from 0.01 to 10 s. *Earthquake Spectra* 2008; **24**(1):139–171.
15. Huang YN, Wittaker AS, Luco N. Maximum spectral demands in the near-fault region. *Earthquake Spectra* 2008; **24**(1):319–341. DOI: 10.1193/1.2830435
16. Shahi SK, Baker JW. NGA-West2 models for ground-motion directionality. *Earthquake Spectra* 2014; (to appear). DOI: 10.1193/040913eqs097m
17. Chiou B, Darragh R, Gregor N, Silva WJ. NGA project strong-motion database. *Earthquake Spectra* 2008; **24**(1):23–44.
18. Bradley BA. Strong ground motion characteristics observed in the 4 September 2010 Darfield, New Zealand earthquake. *Soil Dynamics and Earthquake Engineering* 2012; **42**:32–46. DOI: 10.1016/j.soildyn.2012.06.004
19. McVerry GH, Zhao JX, Abrahamson NA, Somerville PG. New Zealand acceleration response spectrum attenuation relations for crustal and subduction zone earthquakes. *Bulletin of the New Zealand Society for Earthquake Engineering* 2006; **39**(4):1–58.
20. Bradley BA. NZ-specific pseudo-spectral acceleration ground motion prediction equations based on foreign models. *UC Research Report 2010–03*, Department of Civil and Natural Resources Engineering, University of Canterbury, 2010.
21. Bradley BA. A New Zealand-specific pseudospectral acceleration ground motion prediction equation for active shallow crustal earthquakes based on foreign models. *Bulletin of the Seismological Society of America* 2013; **103**(3):1801–1822. DOI: 10.1785/0120120021
22. Gerstenberger M, McVerry G, Rhoades D, Stirling M. Seismic hazard modeling for the recovery of christchurch. *Earthquake Spectra* 2014; **30**(1):17–29.
23. Bradley BA, Quigley MC, van Dissen RJ, Litchfield NJ. Ground motion and seismic source aspects of the Canterbury earthquake sequence. *Earthquake Spectra* 2014; **30**(1):1–15. DOI: 10.1193/030113eqs060m
24. Chiou B, Youngs RR. An NGA Model for the average horizontal component of peak ground motion and response spectra. *Earthquake Spectra* 2008; **24**(1):173–215.
25. Chiou B, Youngs R, Abrahamson N, Addo K. Ground-motion attenuation model for small-to-moderate shallow crustal earthquakes in California and its implications on regionalization of ground-motion prediction models. *Earthquake Spectra* 2010; **26**(4):907–926. DOI: 10.1193/1.3479930
26. Bradley BA. Systematic ground motion observations in the Canterbury earthquakes and region-specific non-ergodic empirical ground motion modeling. *Earthquake Spectra* 2014; (to appear). DOI: 10.1193/053013eqs137m
27. Shahi SK, Baker JW. NGA-West2 models for ground-motion directionality. *PEER report 2013/10*, 2013.
28. Bradley BA, Cubrinovski M. Near-source strong ground motions observed in the 22 February 2011 Christchurch earthquake. *Seismological Research Letters* 2011; **82**(6):853–865. DOI: 10.1785/gssrl.82.6.853
29. Beavan J, Motagh M, Fielding EJ, Donnelly N, Collett D. Fault slip models of the 2010–2011 Canterbury, New Zealand, earthquakes from geodetic data and observations of postseismic ground deformation. *New Zealand Journal of Geology and Geophysics* 2012; **55**(3):207–221. DOI: 10.1080/00288306.2012.697472
30. Bonamassa O, Vidale JE. Directional site resonances observed from aftershocks of the 18 October 1989 Loma Prieta earthquake. *Bulletin of the Seismological Society of America* 1991; **81**(5):1945–1957.